


## SPECIAL ISSUE PAPER

## A novel no-equilibrium hyperchaotic multi-wing system via introducing memristor

Ling Zhou<sup>1,2</sup>, Chunhua Wang<sup>1,\*</sup>  and Lili Zhou<sup>1</sup><sup>1</sup>College of Computer Science and Electronic Engineering, Hunan University, Changsha, China<sup>2</sup>Department of Electronic and Information Engineering, Hunan University of Science and Engineering, Yongzhou, China

## SUMMARY

In this paper, a new multi-wing chaotic attractor is constructed. Based on the proposed multi-wing system, the paper presents a novel method to generate hyperchaotic multi-wing attractors. By introducing a flux-controlled memristor into the proposed multi-wing system, hyperchaotic multi-wing attractor is observed in new memristive system. At the same time, the new memristive system has no equilibrium. The phase portraits and Lyapunov exponents are used to analyze the dynamic behaviors of the no-equilibrium memristive system. Moreover, we analyze the influence on multi-wing system when adding the memristor in different position. The electronic circuit is realized by using off-the-shelf components. Copyright © 2017 John Wiley & Sons, Ltd.

Received 7 June 2016; Revised 9 November 2016; Accepted 12 February 2017

KEY WORDS: no-equilibrium; hyperchaotic; multi-wing; memristor

## 1. INTRODUCTION

After the first hyperchaotic attractor was proposed by Rossler [1], hyperchaotic systems [2–13] characterized by more than one positive Lyapunov exponent (LE) have been extensively researched. Hyperchaotic systems with more complex dynamic behaviors can be used in diverse applications such as cryptosystems [14], neural networks [15], and secure communications [16,17].

The generation of new hyperchaotic attractor has become a hotspot. Lots of hyperchaotic systems have been introduced [2–6]. The common methods for constructing hyperchaotic system can be summarized in the following: One is using state-feedback control and parameter trial-and-error methods to obtain some special types of four- or five-dimensional hyperchaotic systems [2–4]. The other is coupling or parameter perturbation method [5,6].

In 1971, memristor (memory resistor) firstly predicted by L. Chua is a two-terminal nonlinear element [18]. It is not until the fabrication of memristor by TiO<sub>2</sub> in 2008 [19] that the potential applications of memristor have been developed in many realms, such as cellular neural network [20], chaotic system [21], and nonvolatile random access memory [22]. In the realm of nonlinear system, some memristive systems may be hyperchaotic [23,24]. The hyperchaotic systems with double-scroll attractor can be obtained by substituting the nonlinear element with a flux-controlled memristor in canonical Chua's circuit [23] or Murali–Lakshmanan–Chua circuit [24]. However, the method of replacing the nonlinear element with memristor to generate

\*Correspondence to: Chunhua Wang, College of Computer Science and Electronic Engineering, Hunan University, Changsha, 410082 China.

†E-mail: wch1227164@hnu.edu.cn

hyperchaotic attractor cannot work well in all of the systems. In [25–28], these memristive systems can only exhibit normal chaotic behaviors with only one positive LE.

Recently, a flux-controlled memristor is added in 3D chaotic system with double-wing attractor [9,10]; the memristive system is hyperchaotic. Using the same method, the hyperchaotic four-wing system in which an extra cross-product item must be added is proposed [11]. However, the influence of added memristor is not analyzed in the literatures [9–11], and these systems have only two- or four-wing attractor. There are two different classifications in multi-wing systems, which the number of wing is more than two. The one classification is the multi-wing system with smooth nonlinear function [8,11]. The other classification is the multi-wing system with piecewise nonlinear function [12,13,29,30]. In contrast to the chaotic system with double-wing, the multi-wing hyperchaotic system with piecewise nonlinear function possesses the following features: (1) the phase trajectories of multi-wing hyperchaotic attractor can randomly jump in all wings with ergodic property, so that the dynamical behavior is more complicated than those of chaotic system with double-wing, and the statistical properties can be improved [31]; (2) by introducing a nonlinear-function controller, several key parameters of multi-wing chaotic attractors can be easily adjusted, including the width of each segment, amplitude, slope, equilibrium, and turning points. As a result, one can easily control the system equilibrium, the number of wings, the shapes and sizes of the wings, the spatial distribution of the wings, and even the phase trajectories [31]. (3) Hyperchaotic system has better unpredictability, more complex dynamic behavior, and larger key space. Based on previous analysis, the hyperchaotic multi-wing system with piecewise nonlinear function has potential applications in cryptosystem and secure communication. By adding a memristor, the memristive four-wing system with smooth nonlinear function has been discussed in [11]; however, the memristive multi-wing system with piecewise nonlinear function has not been considered. Based on the advantages of the multi-wing hyperchaotic system with piecewise nonlinear function [31], it is interesting and necessary to analyze the memristive multi-wing system with piecewise nonlinear function.

The paper proposes a method to obtain hyperchaotic multi-wing attractor with more complex dynamics by introducing a flux-controlled memristor into the proposed multi-wing system. Compared with the complex coordinate transition and absolute value transition [12] and parameter trial-and-error methods [13], we only need introducing a memristor into the multi-wing system. At the same time, memristor has nanometer size, lower power, and nonlinear characteristics. Moreover, the position of memristor that can affect the new memristive multi-wing system is analyzed. Meanwhile, chaotic attractors without equilibrium, which are considered as hidden attractors, have only bloomed in recent years [32,33]. The identification of hidden attractors is the basis to analyze and control nonlinear dynamical systems with hidden attractors; therefore, studying nonlinear dynamical systems with hidden attractors has academic importance and practical significance. Recently, the multi-scroll (multi-wing) systems without equilibrium are concerned [34–36]. However, they belong to normal chaos. An interesting question ‘Can we construct a no-equilibrium system which can generate hyperchaotic multi-wing chaotic attractors?’ is asked. To the best of our knowledge, there is no literature reported regarding such systems. Hyperchaotic system has more complex dynamic behaviors, and the question that we ask is worth investigating. In this paper, we propose and analyze novel memristive hyperchaotic multi-wing systems with no equilibrium.

The paper is organized as follows. In Section 2, the new multi-wing system is proposed and simulated. In Section 3, the memristive hyperchaotic multi-wing systems and their dynamic behaviors are analyzed. In Section 4, the electronic circuit of no-equilibrium hyperchaotic multi-wing system is realized. Some conclusions are finally given in Section 5.

## 2. THE PROPOSED MULTI-WING SYSTEM

A three-dimensional quadratic double-wing chaotic system is given by

$$\begin{cases} \dot{x} = \alpha(y - x) \\ \dot{y} = y - xz \\ \dot{z} = -\beta + y^2 \end{cases} \tag{1}$$

where  $\alpha = 2$  and  $\beta = 1$  and the numerical simulation results are described in Figure 1.

In order to generate multi-wing attractor in Lorenz-like system, a method based on the extension of saddle-focus equilibrium points with index 2 was proposed [29,37,38]. In these systems, the number of wings was equal to that of saddle-focus equilibrium points with index 2.

In the following section, we adopt the same method for the system (1), and the system with  $2(N + 1)$ -wing can be described as follows:

$$\begin{cases} \dot{x} = \alpha(y - x) \\ \dot{y} = y - xz \\ \dot{z} = f(y) - \beta \end{cases} \tag{2}$$

$$\begin{aligned} f(y) &= F_0 y^2 - \sum_{i=1}^N F_i [1 + 0.5 \operatorname{sgn}(y - E_i) - 0.5 \operatorname{sgn}(y + E_i)] \\ F_0 &= \frac{k}{p} \quad F_i = \frac{2Ap}{k_i} \quad E_i = \frac{0.5(i + 1)Ap}{k} \end{aligned} \tag{3}$$

The nonlinear function  $f(y)$  is the key to generate multi-wing attractor. Letting  $N = 4$ ,  $A = 2$ ,  $p = 1$ ,  $k = 1$ ,  $k_1 = 0.8$ ,  $k_2 = 0.8$ ,  $k_3 = 0.6$ , and  $k_4 = 0.45$ , it can be obtained that  $F_0 = 1$ ,  $F_1 = 5$ ,  $F_2 = 5$ ,  $F_3 = 6.67$ ,  $F_4 = 8.89$ ,  $E_1 = 2$ ,  $E_2 = 3$ ,  $E_3 = 4$ , and  $E_4 = 5$ . The numerical simulation results of multi-wing chaotic attractors are depicted in Figure 2 when  $N = 4$ .

It is easy to see that the system (2) is invariant under the transformation  $(x, y, z) \leftrightarrow (-x, -y, z)$  with  $z$ -axis symmetry.

When  $i = 0, 1, 2, \dots, N$ , the equilibrium points with index 1 (expressed as  $(v_{\pm i}, v_{\pm i}, 1)$ , where  $v_{\pm i} = \pm 0.5 (1 + i)Ap/k$ , and marked with ‘ $\square$ ’ in Figure 3) are not essential. The second type of equilibrium points (marked with ‘ $\circ$ ’ in Figure 3) is main consideration, and they can be described as  $(u_{\pm i}, u_{\pm i}, 1)$ .

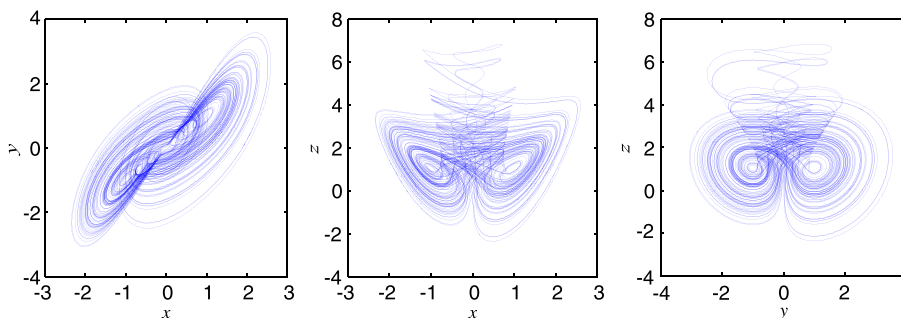


Figure 1. Simulated phase portraits of system (1) under the initial condition  $[0, 0.1, 0]$ : (a)  $x$ - $y$  plane; (b)  $x$ - $z$  plane; (c)  $y$ - $z$  plane. [Colour figure can be viewed at [wileyonlinelibrary.com](http://wileyonlinelibrary.com)]

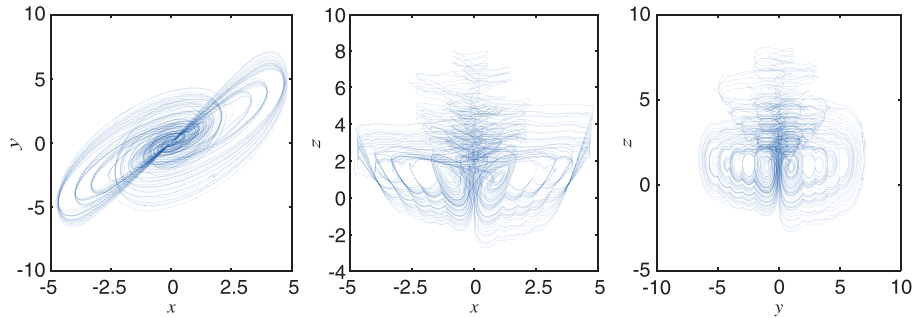


Figure 2. Simulated phase portraits of system (2) under the initial condition  $[0, 0.1, 0]$ : (a)  $x$ - $y$  plane; (b)  $x$ - $z$  plane; (c)  $y$ - $z$  plane. [Colour figure can be viewed at [wileyonlinelibrary.com](http://wileyonlinelibrary.com)]

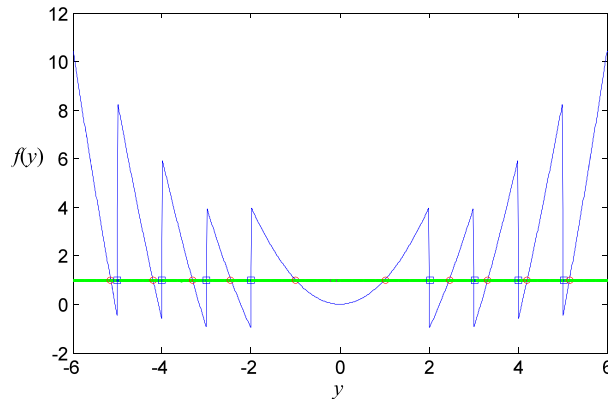


Figure 3. The equilibrium points  $(u_{\pm i}, u_{\pm i}, 1)$  in system (2) when  $N = 4$ . [Colour figure can be viewed at [wileyonlinelibrary.com](http://wileyonlinelibrary.com)]

$$u_{\pm i} = \begin{cases} \pm \sqrt{\beta/F_0} & i = 0 \\ \pm \sqrt{\frac{\beta + \sum_{i=1}^N F_i}{F_0}} & 1 \leq i \leq N \end{cases} \quad (4)$$

When  $N = 4$ , there are  $2(N + 1) = 10$  equilibrium points with index 2, which can be derived as

$$\begin{aligned} Q_{\pm 0}(\pm 1, \pm 1, 1) \\ Q_{\pm 1}(\pm 2.4495, \pm 2.4495, 1) \\ Q_{\pm 2}(\pm 3.3166, \pm 3.3166, 1) \\ Q_{\pm 3}(\pm 4.2036, \pm 4.2036, 1) \\ Q_{\pm 4}(\pm 5.1536, \pm 5.1536, 1) \end{aligned} \quad (5)$$

By linearizing the system (2), the Jacobian matrix is

$$J_{-Q_{\pm i}} = \begin{bmatrix} -\alpha & \alpha & 0 \\ -z & 1 & -x \\ 0 & 2F_0 y & 0 \end{bmatrix}_{Q_{\pm i}} \quad i = 0, 1, 2, \dots, N \quad (6)$$

The corresponding eigenvalues of each equilibrium point in (5) are obtained as follows:

$$\begin{aligned}
 \gamma_{\pm 0} &= -1.4780 & \sigma_{\pm 0} \pm j\omega_{\pm 0} &= 0.2390 \pm j1.6277 \\
 \gamma_{\pm 0} &= -1.4780 & \sigma_{\pm 0} \pm j\omega_{\pm 0} &= 0.2390 \pm j1.6277 \\
 \gamma_{\pm 0} &= -1.4780 & \sigma_{\pm 0} \pm j\omega_{\pm 0} &= 0.2390 \pm j1.6277 \\
 \gamma_{\pm 0} &= -1.4780 & \sigma_{\pm 0} \pm j\omega_{\pm 0} &= 0.2390 \pm j1.6277 \\
 \gamma_{\pm 0} &= -1.4780 & \sigma_{\pm 0} \pm j\omega_{\pm 0} &= 0.2390 \pm j1.6277
 \end{aligned}
 \tag{7}$$

The LEs are 0.317662,  $-0.001242$ , and  $-1.316417$ . Therefore, the system is normal chaos. And the circuit diagram of system (2) is shown in Figure 4.

### 3. THE MEMRISTIVE HYPERCHAOTIC MULTI-WING SYSTEM

#### 3.1. The memristor

Memristor can be classified as charge-dependent and flux-dependent memristor. The memristor used in this paper is a flux-controlled memristor. The relationship between voltage and current of flux-controlled memristor can be expressed as

$$i_m = W(\varphi)v, \quad \dot{\varphi} = \kappa v \tag{8}$$

where  $W(\varphi)$  is an incremental memductance function [18]. Various mathematical models and emulator circuits have been reported [39–42] in order to research the characteristics and application of memristor. The memductance function frequently used in nonlinear systems [9–11,43–45] is given by

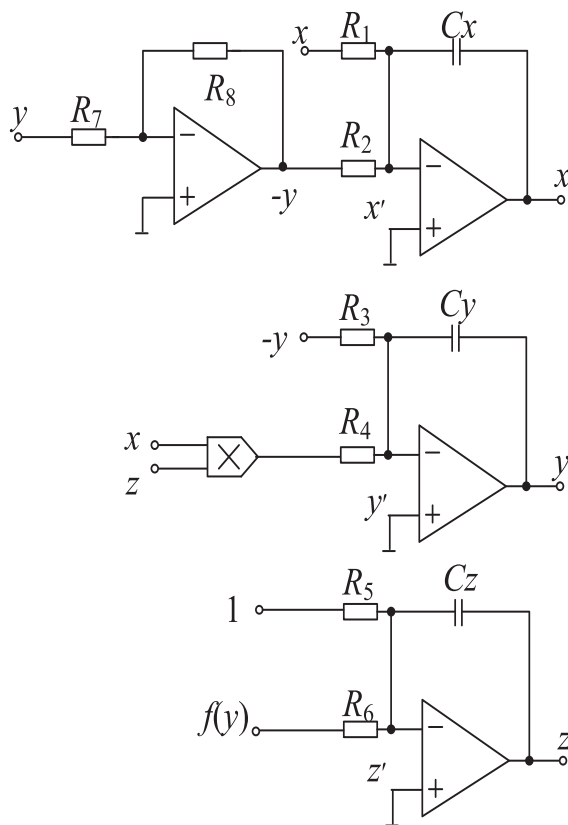


Figure 4. The circuit diagram of system (2) with 2(N + 1)-wing.

$$W(\varphi) = dq(\varphi)/d\varphi = a + 3b\varphi^2 \tag{9}$$

where  $a$  and  $b$  are two positive constants.

3.2. The memristive multi-wing systems and their dynamic characteristics

To obtain hyperchaotic multi-wing attractor, a flux-controlled memristor is added in the proposed multi-wing system. The implementation circuit can be presented in Figure 5.

From (8) and Figure 5, it can be obtained that

$$\begin{cases} C_x \dot{v}_x = v_y/R_2 - v_x/R_1 - W(\varphi)(-v_x) \\ C_y \dot{v}_y = v_y/R_3 - v_x v_z/R_4 \\ C_z \dot{v}_z = f(y)/R_5 - 1/R_6 \\ C_\varphi \dot{v}_\varphi = \kappa(-v_x) \end{cases} \tag{10}$$

where  $v_x, v_y, v_z, -v_x, -v_y,$  and  $-v_z$  respectively indicate the voltage of  $x, y, z, -x, -y,$  and  $-z$ .

Let  $t = \tau RC$ , where  $\tau$  is the dimensionless time. When choosing the parameters expressed as follows:  $C_x = C_y = C_z = C, a = R/R_1 = R/R_2, R_3 = R_4 = R_5 = R_6 = R,$  the dimensionless equations can be described as follows:

$$\begin{cases} \dot{x} = \alpha(y - x) + \rho W(\varphi)x \\ \dot{y} = y - xz \\ \dot{z} = f(y) - 1 \\ \dot{\varphi} = -\kappa x \end{cases} \tag{11}$$

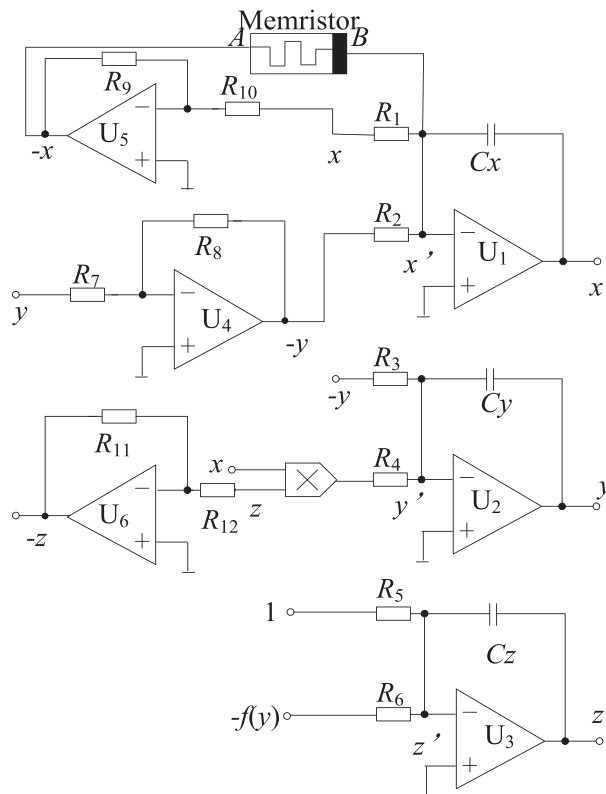


Figure 5. The circuit implementation after adding an extra memristor.

where  $\rho$  is a coefficient of the term containing memristor in (11), and we consider  $\rho > 0$  in the following paper.

Compared with (2), it is easy to see that the memristive system (11) is invariant under the transformation  $(x, y, z, \varphi) \leftrightarrow (-x, -y, z, -\varphi)$  with  $z$ -axis symmetry.

The equilibrium for system (11) is obtained by

$$\alpha(y - x) + \rho W(\varphi)x = 0 \quad (12)$$

$$y - xz = 0 \quad (13)$$

$$f(y) - 1 = 0 \quad (14)$$

$$\kappa x = 0 \quad (15)$$

From (12) and (15), we obtain that  $x = y = 0$ , which is inconsistent with (14). Therefore, there is no equilibrium in the system (11).

The question ‘what happen if the position of memristor changes’ is fascinating. We will discuss the question in the following.

The nodes  $x, y, z, -x, -y, -z, x', y',$  and  $z'$  are marked in Figure 5. Terminal A of memristor can connect to one of nodes  $x, y, z, -x, -y,$  and  $-z$ , and terminal B of memristor can connect to one of nodes  $x', y'$  and  $z'$ . Therefore, there are different situations for the connection of memristor.

Based on the previous analysis, the positions of added memristor are discussed, and their dynamic behaviors are analyzed in Table I (when the connection way is  $xx', xy', xz', yx', yy', yz', zx', zy',$  and  $zz'$ , the similar analysis can also be obtained, and here, we do not list the table), where the connection way  $-xx'$  indicates the Case when terminal A of memristor connects node  $-x$  and terminal B connects node  $x'$ , and the connection way  $-xy'$  indicates the Case when terminal A of memristor connects node  $-x$  and terminal B connects node  $y'$  and so on.

There is all no equilibrium in the every memristive system in Table I. It is worth noting that the chaotic system without equilibrium is categorized as that with hidden attractor. In the following, the phase portraits and LEs are analyzed when the parameters are taken as  $\alpha = 2, \beta = 1,$  and  $\kappa = 0.1$ .

### 3.3. The phase portraits and Lyapunov exponents

The phase portraits and LEs are main tools to analyze dynamic behavior. The possible Cases when adding an extra memristor are analyzed. It is found that there are chaotic attractors in Cases 7–9 only when the parameter  $\rho$  is very small ( $\rho \approx 0.0001$ ), and the common of these cases is that terminal A of memristor is connected to node  $-z$ . Therefore, Cases 7–9 are not considered.

**3.3.1. Lyapunov exponents.** The sign function  $\text{sgn}(x \pm Ei)$ , which is non-differentiable at zero, is replaced by the continuous differentiable function  $\tanh(K_0(x \pm Ei))$  in order to calculate the LEs [7,13]. In general, the bigger the parameter  $K_0$ , the better the approximate performance, so we choose  $K_0 = 1000$ . We take the Dormand–Prince method (RK45) as the ODEs solver and use the famous Wolf method. The LEs are calculated in Cases 1–3, and the initial condition is  $[0 \ 0.1 \ 0 \ 0]$ . The numerical results are depicted in Figure 6 (The last one is not displayed because it is always a big negative number).

From Figure 6, the hyperchaotic attractors are discovered in Cases 1–2 and Cases 4–5. The LEs and memristor’s parameters are shown in Table II. Unfortunately, nothing hyperchaotic attractors are observed in Cases 2 and 3.

Table I. Dynamic analysis of new memristive systems in different connection way.

Case	Connection way	Dimensionless equation	Symmetry
Case 1	$-xx'$	$\begin{cases} \dot{x} = \alpha(y - x) + \rho W(\varphi)x \\ \dot{y} = y - xz \\ \dot{z} = f(y) - \beta \\ \dot{\varphi} = -\kappa x \end{cases}$	$(x, y, z, \varphi) \leftrightarrow (-x, -y, z, -\varphi)$ with $z$ -axis symmetry
Case 2	$-xy'$	$\begin{cases} \dot{x} = \alpha(y - x) \\ \dot{y} = y - xz + \rho W(\varphi)x \\ \dot{z} = f(y) - \beta \\ \dot{\varphi} = -\kappa x \end{cases}$	$(x, y, z, \varphi) \leftrightarrow (-x, -y, z, -\varphi)$ with $z$ -axis symmetry
Case 3	$-xz'$	$\begin{cases} \dot{x} = \alpha(y - x) \\ \dot{y} = y - xz \\ \dot{z} = f(y) + \rho W(\varphi)x - \beta \\ \dot{\varphi} = -\kappa x \end{cases}$	no
Case 4	$-yx'$	$\begin{cases} \dot{x} = \alpha(y - x) + \rho W(\varphi)y \\ \dot{y} = y - xz \\ \dot{z} = f(y) - \beta \\ \dot{\varphi} = -\kappa y \end{cases}$	$(x, y, z, \varphi) \leftrightarrow (-x, -y, z, -\varphi)$ with $z$ -axis symmetry
Case 5	$-yy'$	$\begin{cases} \dot{x} = \alpha(y - x) \\ \dot{y} = y - xz + \rho W(\varphi)y \\ \dot{z} = f(y) - \beta \\ \dot{\varphi} = -\kappa y \end{cases}$	$(x, y, z, \varphi) \leftrightarrow (-x, -y, z, -\varphi)$ with $z$ -axis symmetry
Case 6	$-yz'$	$\begin{cases} \dot{x} = \alpha(y - x) \\ \dot{y} = y - xz \\ \dot{z} = f(y) + \rho W(\varphi)y - \beta \\ \dot{\varphi} = -\kappa y \end{cases}$	no
Case 7	$-zx'$	$\begin{cases} \dot{x} = \alpha(y - x) + \rho W(\varphi)z \\ \dot{y} = y - xz \\ \dot{z} = f(y) - \beta \\ \dot{\varphi} = -\kappa z \end{cases}$	no
Case 8	$-zy'$	$\begin{cases} \dot{x} = \alpha(y - x) \\ \dot{y} = y - xz + \rho W(\varphi)z \\ \dot{z} = f(y) - \beta \\ \dot{\varphi} = -\kappa z \end{cases}$	no
Case 9	$-zz'$	$\begin{cases} \dot{x} = \alpha(y - x) \\ \dot{y} = y - xz \\ \dot{z} = f(y) + \rho W(\varphi)z - \beta \\ \dot{\varphi} = -\kappa z \end{cases}$	$(x, y, z, \varphi) \leftrightarrow (-x, -y, z, \varphi)$

3.3.2. *The phase portraits.* The question whether the extra memristor affect the multi-wing properties will be asked. It is easy to observe the multi-wing properties from phase portraits.

*Case 1*

The phase portraits are shown in Figure 7 when the initial condition is [0 0.1 0 0] and the parameters are taken as  $a = 0.65$ ,  $b = 1/30$ ,  $\rho = 0.24$ ,  $\alpha = 2$ ,  $\beta = 1$ , and  $\kappa = 0.1$ .



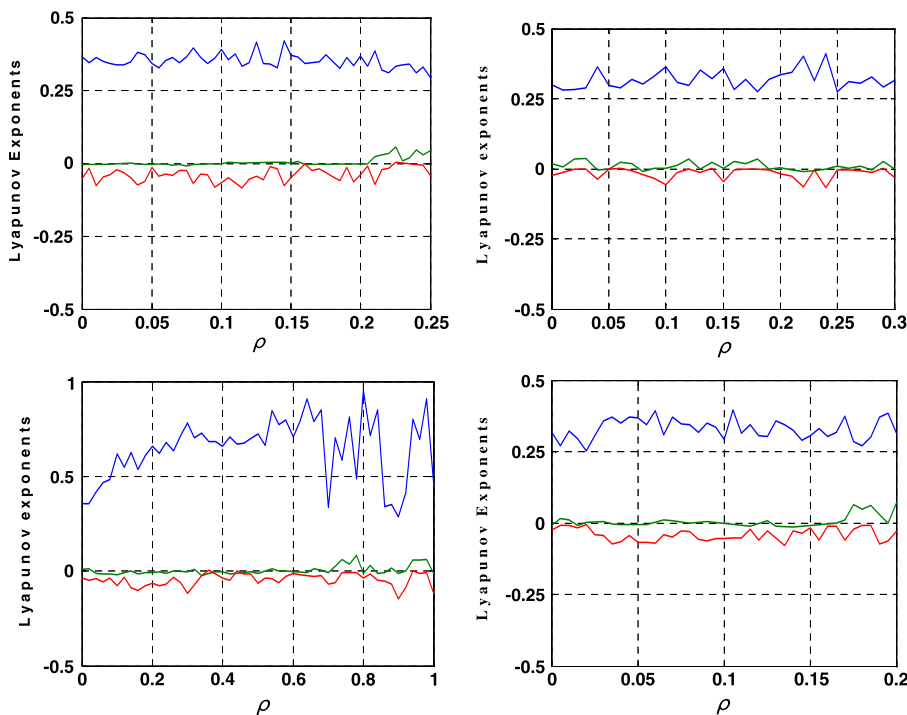


Figure 6. First three Lyapunov exponents of memristive multi-wing systems in different cases: (a) Case 1; (b) Case 2; (c) Case 4; (d) Case 5. [Colour figure can be viewed at wileyonlinelibrary.com]

Table II. The Lyapunov exponents (LEs) and memristor’s parameters.

Case	Memristor’s parameter	LEs
Case 1	$a = 0.65, b = 1/30, \rho = 0.24$	0.311267, 0.046489, $-0.009402, -1.005634$
Case 2	$a = 0.5, b = 1/12, \rho = 0.12$	0.290539, 0.044846, 0.000096, $-1.335481$
Case 4	$a = 20, b = 2/3, \rho = 0.94$	0.807309, 0.088699, $-0.0023575, -1.872436$
Case 5	$a = 1, b = 0.1, \rho = 0.18$	0.271676, 0.049507, $-0.003803, -0.729386$

The similar multi-wing attractors are also observed in Case 2, Case 4, and Case 5. We will not enumerate here.

Case 3

The phase portraits are shown in Figure 8 when the initial condition is  $[0 \ 0.1 \ 0 \ 0]$  and the parameters are taken as  $a = 0.3, b = 1/30, \rho = 0.1, \alpha = 2, \beta = 1,$  and  $\kappa = 0.1$ .

Case 6

The phase portraits are shown in Figure 9 when the initial condition is  $[0 \ 0.1 \ 0 \ 0]$  and the parameters are taken as  $a = 3, b = 1/30, \rho = 0.1, \alpha = 2, \beta = 1,$  and  $\kappa = 0.1$ .

From Figures 8 and 9, the symmetry of multi-wing attractor is destroyed. From Table I, the two Cases have something in common, and terminal B of memristor is connected to node  $z'$ . From the dimensionless equation, the added terms  $\rho w(\varphi)x$  and  $\rho w(\varphi)y$  in the third equation destroy the nonlinear function  $f(y)$ .

Based on the previous analysis, it can be observed that these no-equilibrium memristive systems in Cases 1–2 and Cases 4–5 have good hyperchaotic multi-wing attractors. From Table I, these Cases are all with  $z$ -axis symmetry. Therefore, we can conclude the steps to construct hyperchaotic multi-wing attractor by adding memristor. Firstly, we should analyze the symmetry of original multi-wing

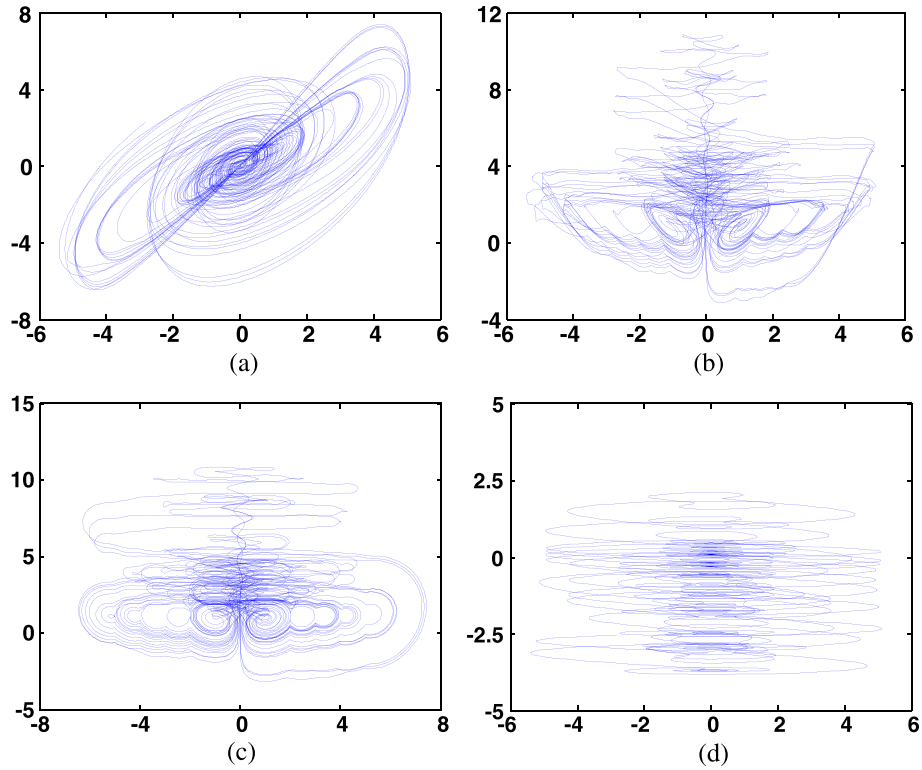


Figure 7. The phase portraits in Case 1: (a)  $x$ - $y$  plane; (b)  $x$ - $z$  plane; (c)  $y$ - $z$  plane; (d)  $x$ - $\phi$  plane. [Colour figure can be viewed at [wileyonlinelibrary.com](http://wileyonlinelibrary.com)]

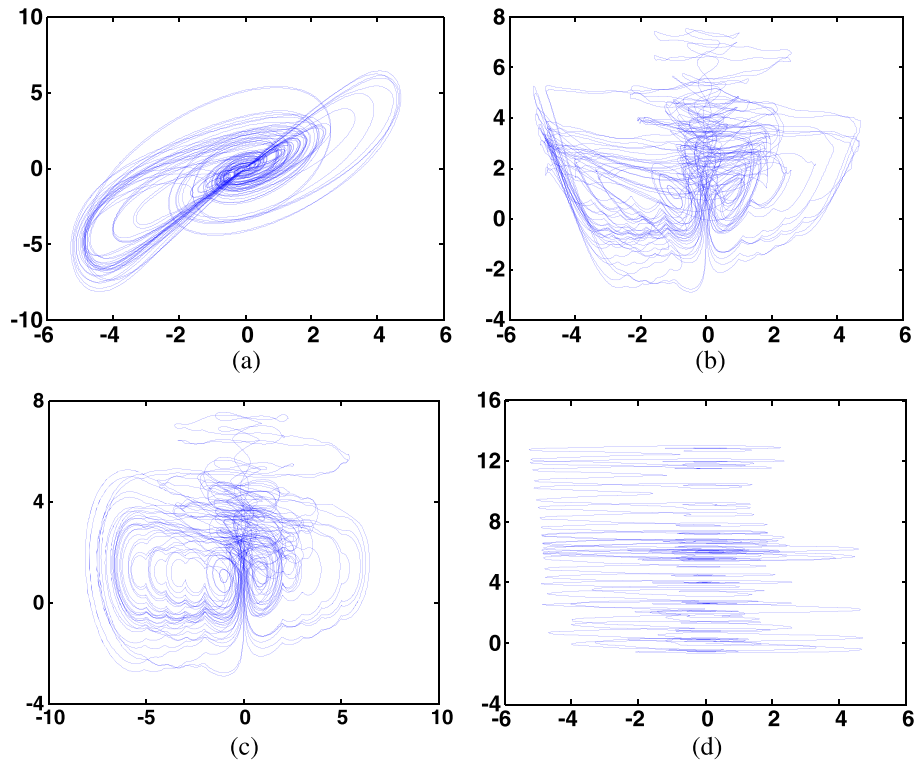


Figure 8. The phase portraits in Case 2: (a)  $x$ - $y$  plane; (b)  $x$ - $z$  plane; (c)  $y$ - $z$  plane; (d)  $x$ - $\phi$  plane. [Colour figure can be viewed at [wileyonlinelibrary.com](http://wileyonlinelibrary.com)]

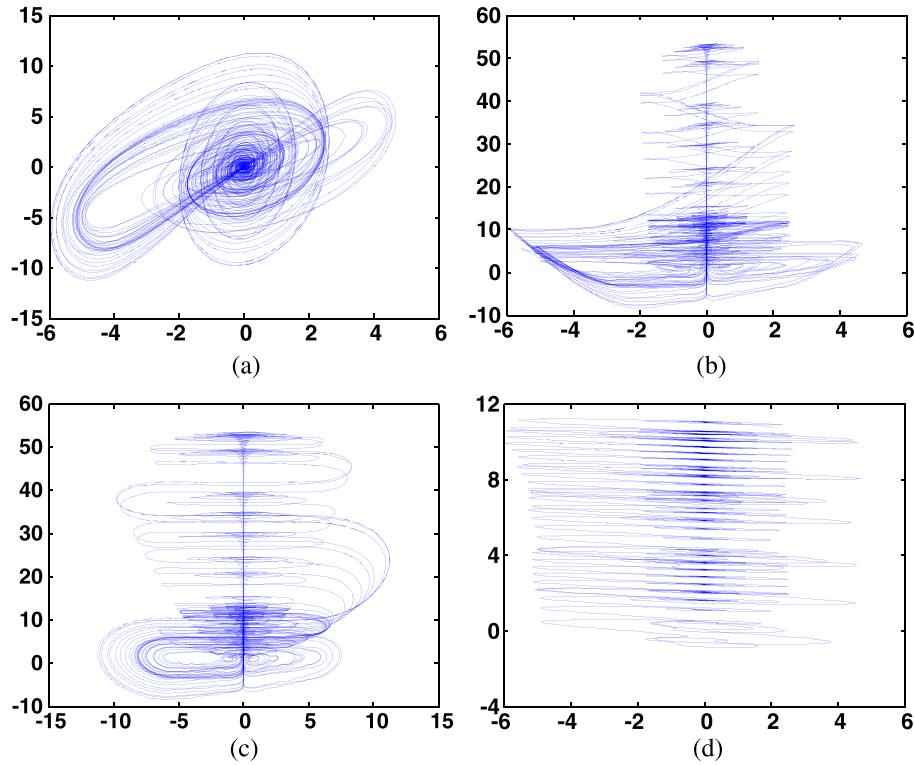


Figure 9. The phase portraits in Case 3: (a)  $x$ - $y$  plane; (b)  $x$ - $z$  plane; (c)  $y$ - $z$  plane; (d)  $x$ - $\varphi$  plane. [Colour figure can be viewed at [wileyonlinelibrary.com](http://wileyonlinelibrary.com)]

chaotic system. Then, we add the memristor to original system, and the symmetry of new memristive multi-wing system is according to that of original system. At last, we only adjust the parameter  $\rho$  to construct hyperchaotic multi-wing system.

#### 4. CIRCUIT IMPLEMENTATION

In order to further survey the no-equilibrium hyperchaotic multi-wing attractor, we take Case 1 when the connection way of memristor is  $-xx'$  as an example. The electronic circuit using operational amplifiers TL082 and multipliers AD633JN is realized. Their supply voltages are  $E = \pm 15$  V, and their saturated voltages are  $V_{\text{sat}} \approx \pm 13.5$  V. From Figure 7, the values of  $x$ ,  $y$ ,  $z$ , and  $\varphi$  are in the dynamic range, so it is not necessary to rescale the state variables.

Let  $t = \tau RC$ , where  $\tau$  is the dimensionless time.  $R$  is a reference resistor, and  $C$  is a reference capacitor. Substituting (9) into (11), and it can be described by

$$\begin{cases} RC \frac{dx}{dt} = \alpha(y - x) + \rho(a + 3b\varphi^2)x \\ RC \frac{dy}{dt} = y - xz \\ RC \frac{dz}{dt} = f(y) - 1 \\ RC \frac{d\varphi}{dt} = -\kappa x \end{cases} \quad (16)$$

Similar to [9,10], a simple memristor model with off-the-shelf components is described in Figure 10 (a). It can be obtain that

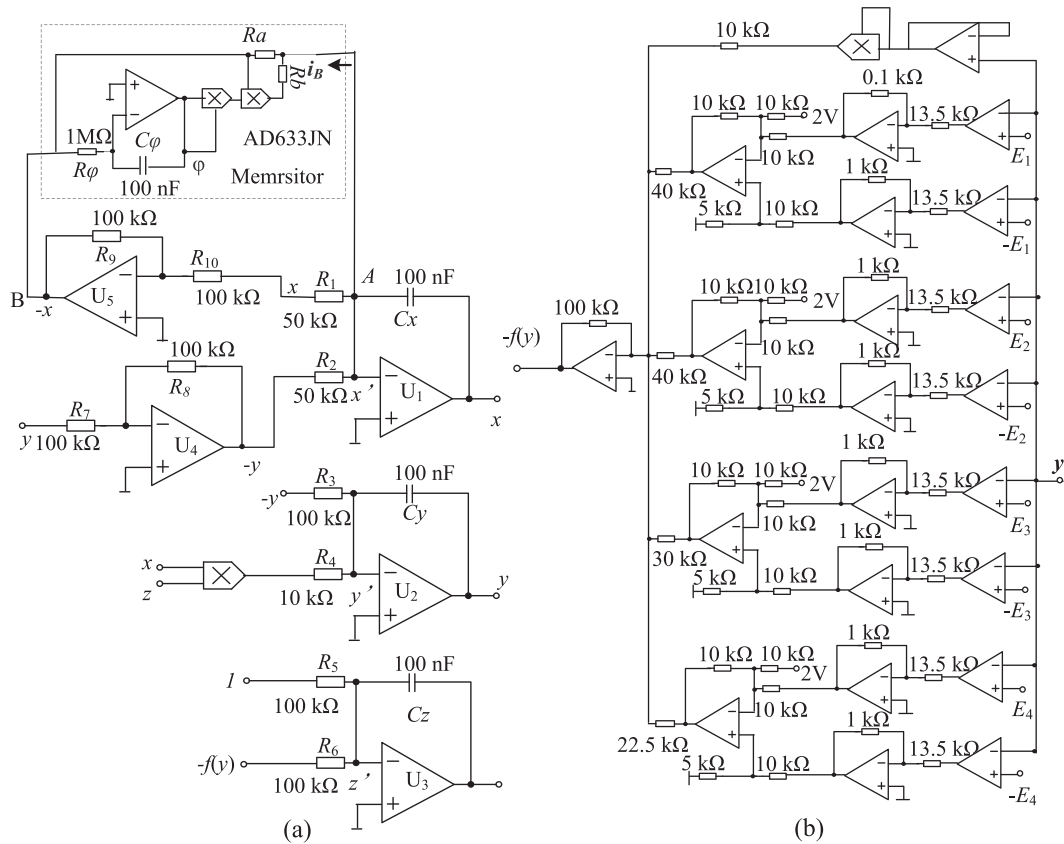


Figure 10. The schematic (a) circuit implementation of system (16) in Case 1; (b) circuit implement of function  $-f(y)$ .

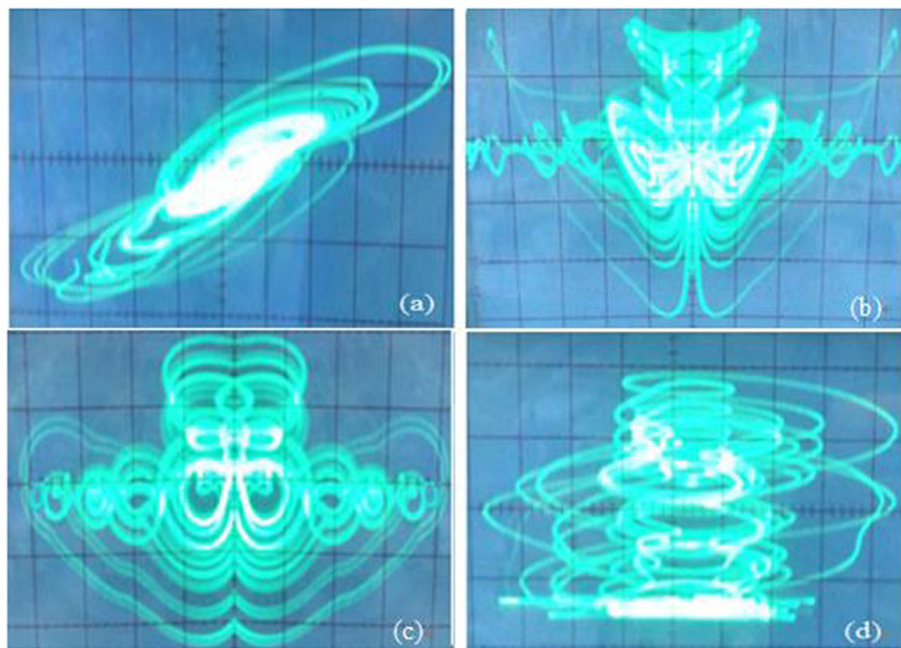


Figure 11. Experimental observations of memristive hyperchaotic multi-wing system. (a)  $x$ - $y$  plane; (b)  $x$ - $z$  plane; (c)  $y$ - $z$  plane; (d)  $x$ - $\phi$  plane. [Colour figure can be viewed at [wileyonlinelibrary.com](http://wileyonlinelibrary.com)]

$$i_B = w(\varphi)(-v_x) = \frac{-v_x}{R_a} + \frac{v_\varphi^2(-v_x)}{R_b} \quad (17)$$

where  $i_B$  is the input current of the memristor.

By putting a multiplication factor  $0.1/V$  of multiplier AD633JN and substituting (17) into (10), Equation (10) can be rewrote as follows:

$$\begin{cases} C_x \frac{v_x}{dt} = v_y/R_2 - v_x/R_1 - \left[ \frac{-v_x}{R_a} + \frac{(v_\varphi v_\varphi \cdot 0.1/V)(-v_x) \cdot 0.1/V}{R_b} \right] \\ C_y \frac{v_y}{dt} = v_y/R_3 - v_x v_z \cdot 0.1V/R_4 \\ C_z \frac{v_z}{dt} = f(y)/R_5 - 1/R_6 \\ C_\varphi \frac{v_\varphi}{dt} = (-v_x)/R_\varphi \end{cases} \quad (18)$$

where  $v_x$ ,  $v_y$ ,  $v_z$ , and  $v_\varphi$  are the voltages on capacitors.

Compared (16) with (18), the parameters are taken as follows:

$C_x = C_y = C_z = C_\varphi = C$ ,  $R_1 = R_2 = R/a$ ,  $R_4 = 0.1R$ ,  $R_3 = R_5 = R_6 = R_7 = R_8 = R_9 = R_{10} = R$ ,  $R_\varphi = 10R$ ,  $R_a = R/(\rho a)$ ,  $R_b = R/(300\rho b)$ .

Now, let us take  $R = 100 \text{ k}\Omega$  and  $C = 100 \text{ nF}$ . According to the parameters of the original system and Table I, that is,  $\alpha = 2$ ,  $\beta = 1$ ,  $\kappa = 0.1$ ,  $a = 0.65$ ,  $b = 1/30$ , and  $\rho = 0.24$ , so  $R_1 = R_2 = 50 \text{ k}\Omega$ ,  $R_4 = 10 \text{ k}\Omega$ ,  $R_3 = R_5 = R_6 = R_7 = R_8 = R_9 = R_{10} = 100 \text{ k}\Omega$ ,  $R_a = 641 \text{ K}\Omega$ , and  $R_b = 41.67 \text{ k}\Omega$ . The schematic of system (10) is shown in Figure 10.

Figure 11 shows the oscilloscope traces from this no-equilibrium memristive multi-wing circuit in Figure 10. It can be observed that the results in Figure 11 are in agreement with Figure 7.

## 5. CONCLUSION

A novel hyperchaotic multi-wing system, which has no equilibrium, has been introduced by adding a flux-controlled memristor in the proposed multi-wing system. Moreover, we conclude the steps to construct memristive multi-wing system; and this method of adding extra flux-controlled memristor can be extended to design and implement other new continuous hyperchaotic multi-wing or grid multi-wing systems. The theoretical analysis, numerical simulation, and circuit implementation of new memristive multi-wing systems are realized in order to research the new systems.

## ACKNOWLEDGEMENTS

This work is supported by the National Natural Science Foundation of China (nos 61571185 and 61274020), the Natural Science Foundation of Hunan Province, China (no. 2016JJ2030), the Open Fund Project of Key Laboratory in Hunan Universities (no. 15K027), and the science and technology planned project of Yongzhou City.

## REFERENCES

1. Rossler O. An equation for hyperchaos. *Physics Letters A* 1979; **71**(2):155–157.
2. Chen A, Lü JH, Yu S. Generating hyperchaotic Lü attractor via state feedback control. *Physica A* 2006; **364**:103–110.
3. Hu G. Generating hyperchaotic attractors with three positive Lyapunov exponents via state feedback control. *International Journal of Bifurcation and Chaos* 2009; **19**(2):651–660.
4. Hu G. Hyperchaos of higher order and its circuit implementation. *International Journal of Circuit Theory and Applications* 2011; **39**(1):79–89.
5. Giuseppe G, Frank LS, Damon AM. Multi-wing hyperchaotic attractors from coupled Lorenz systems. *Chaos, Solitons & Fractals* 2009; **41**:284–291.
6. Tam LM, Chen JH, Chen HK, Tou WMS. Generation of hyperchaos from the Chen-Lee system via sinusoidal perturbation. *Chaos, Solitons & Fractals* 2008; **38**(3):826–839.

7. Li CB, Sprott JC, Thio W, Zhu HQ. A new piecewise linear hyperchaotic circuit. *IEEE Transaction on Circuits System Part II: Express Briefs* 2014; **61**(12):977–981.
8. Li Y, Tang WKS, Chen G. Complex dynamics in a 5-D hyper-chaotic attractor with four-wing, one equilibrium and multiple chaotic attractors. *Nonlinear Dynamics* 2015; **81**:585–605.
9. Li QD, Zeng HZ, Li J. Hyperchaos in a 4D memristive circuit with infinitely many stable equilibria. *Nonlinear Dynamics* 2015; **79**:2295–2308.
10. Li QD, Hu SY, Tang S, Zeng G. Hyperchaos and horseshoe in a 4D memristive system with a line of equilibria and its implementation. *International Journal of Circuit Theory and Applications* 2014; **42**:1172–1188.
11. Ma J, Chen ZQ, Wang ZL, Zhang Q. A four-wing hyper-chaotic attractor generated from a 4-D memristive system with a line equilibrium. *Nonlinear Dynamics* 2015; **81**(3):1275–1288.
12. Yu B, Hu GS. Constructing multi-wing hyperchaotic attractors. *International Journal of Bifurcation and Chaos* 2010; **20**(3):727–734.
13. Zhang CX, Yu SM. On constructing complex grid multi-wing hyperchaotic system: theoretical design and circuit implementation. *International Journal of Circuit Theory and Applications* 2013; **38**:221–237.
14. Wu XJ, Bai CX, Kan HB. A new color image cryptosystem via hyperchaos synchronization. *Communications in Nonlinear Science and Numerical Simulation* 2014; **6**(19):1884–1897.
15. Swathy PS, Thamilaran K. Hyperchaos in SC-CNN based modified canonical Chua's circuit. *Nonlinear Dynamics* 2014; **4**(78):2639–2650.
16. Rania LF, Mohamed B, Pierre B. On observer-based secure communication design using discrete-time hyperchaotic systems. *Communications in Nonlinear Science and Numerical Simulation* 2014; **19**(5):1424–1432.
17. Sadoudi S, Tanougast C, Azzaz MS, Dandache A. Design and FPGA implementation of a wireless hyperchaotic communication system for secure realtime image transmission. *EURASIP Journal on Image and Video Processing* 2013; **43**:1–18.
18. Chua LO. Memristor – the missing circuit element. *IEEE Transaction on Circuit Theory* 1971; **18**:507–519.
19. Strukov DB, Snider GS, Stewart DR, Williams RS. The missing memristor found. *Nature* 2008; **453**:80–83.
20. Duan SK, Hu XF, Dong ZK, Wang LD, Mazumder P. Memristor-based cellular nonlinear/neural network: design, analysis, and applications. *IEEE Transactions on neural networks and learning systems* 2015; **26**(6):1202–1213.
21. Rakkiyappan R, Sivasamy R, Xd L. Synchronization of identical and nonidentical memristor-based chaotic systems via active backstepping control technique. *Circuits System and Signal Process* 2015; **34**:763–778.
22. Sarwar SS, Saqueeb SAN, Quaiyum F, Harun-Ur Rashid, ABM. Memristor-based nonvolatile random access memory: hybrid architecture for low power compact memory design. *IEEE Access* 2013; **1**:29–34.
23. Fitch AL et al. Hyperchaos in a memristor-based modified canonical chua's circuit. *International Journal of Bifurcation and Chaos* 2012; **22**(6):1250133.
24. Ishaq A, Ahamed LM. Nonsmooth bifurcations, transient hyperchaos and hyperchaotic beats in memristive murali-lakshmanan-chua circuit. *International Journal of Bifurcation and Chaos* 2013; **23**(6):1350098-1-28.
25. Bao BC et al. A simple memristor chaotic circuit with complex dynamics. *International Journal of Bifurcation and Chaos* 2011; **21**(9):2629–2645.
26. Buscarino A et al. Memristive chaotic circuits based on cellular nonlinear networks. *International Journal of Bifurcation and Chaos* 2012; **22**(3):1250070.
27. Itoh M, Chua LO. Memristor oscillators. *International Journal of Bifurcation and Chaos* 2008; **18**(11):3183–3206.
28. El-Sayed A et al. Dynamical behavior, chaos control and synchronization of a memristor-based ADVP circuit. *Communications in Nonlinear Science and Numerical Simulation* 2013; **18**(1):148–170.
29. Zhang CX, Yu SM, Zhang Y. Design and realization of multi-wing butterfly chaotic attractors via switching control. *International Journal of Modern Physics B* 2011; **25**(16):2183–2194.
30. Wang ZL, Tang H, Chen ZQ. The design and implementation of a multi-wing chaotic attractor based on a five-term three-dimension system. *International Journal of Circuit Theory and Applications* 2016; **44**(5):1186–1201.
31. Zhang CX, Yu SM. A novel methodology for constructing a multi-wing chaotic and hyperchaotic system with a unified step function switching control. *Chinese Physics B* 2016; **25**(5):050503.
32. Wei Z. Dynamical behaviors of a chaotic system with no equilibria. *Physics Letters A* 2011; **376**(2):102–108.
33. Leonov GA, Kuznetsov NV, Vagaitsev VI. Hidden attractor in smooth Chua systems. *Physica D* 2012; **241**(18):1482–1486.
34. Jafari S, Pham VT, Kapitaniak T. Multiscroll chaotic sea obtained from a simple 3d system without equilibrium. *International Journal of Bifurcation and Chaos* 2016; **26**(02):1650031.
35. Hu XY, Liu CX, Liu L, Ni JK, Li SL. Multi-scroll hidden attractors in improved Sprott A system. *Nonlinear Dynamics* 2016; **86**(3):1725–1734.
36. Tahir FR, Jafari S, Pham VT, Volos C, Wang X. A novel no-equilibrium chaotic system with multiwing butterfly attractors. *International Journal of Bifurcation and Chaos* 2015; **25**(04):1550056.
37. Yu SM, Wallace Tang KS, Lu JH, Chen GR. Design and implementation of multi-wing butterfly chaotic attractors via Lorenz-type systems. *International Journal of Bifurcation and Chaos* 2010; **20**(1):29–41.
38. Yu SM, Tang WKS, Lu JH, Chen GR. Generating 2n-wing attractors from Lorenz-like systems. *International Journal of Circuit Theory and Applications* 2010; **38**:243–258.
39. Ascoli A, Corinto F, Tetzlaff R. Generalized boundary condition memristor model. *International Journal of Circuit Theory and Applications* 2016; **44**(1):60–84.



40. Di Ventra M, Pershin YV, Chua LO. Circuit elements with memory: memristors, memcapacitors, and meminductors. *Proceedings of the IEEE* 2009; **97**(10):1717–1724.
41. Corinto F, Ascoli A. Memristive diode bridge with LCR filter. *Electronics Letters* 2012; **48**(14):824–825.
42. Secco J, Biey M, Corinto F, Ascoli A, Tetzlaff R. Complex behavior in memristor circuits based on static nonlinear two-ports and dynamic bipole. *2015 European Conference on Circuit Theory and Design (ECCTD)*. Trondheim, Norway, 2015; 1–4.
43. Muthuswamy B. Implementing memristor based chaotic circuits. *International Journal of Bifurcation and Chaos* 2010; **20**(5):1335–1350.
44. Iu HHC, Yu DS, Fitch AL, Sreeram V, Chen H. Controlling chaos in a memristor based circuit using a Twin-T notch filter. *IEEE Transaction on Circuits System Part I: Regular Papers* 2011; **58**(6):1337–1344.
45. Bao BC, Xu JP, Zhou G, Ma ZH, Zou L. Chaotic memristive circuit: equivalent circuit realization and dynamical analysis. *Chinese Physics B* 2011; **20**(12):120502-1–7.